Journal of Power Sources 195 (2010) 4893–4904

Contents lists available at ScienceDirect

Journal of Power Sources

journal homepage: www.elsevier.com/locate/jpowsour

Comparison of the multicomponent mass transfer models for the prediction of the concentration overpotential for solid oxide fuel cell anodes

Yasemin Vural*, Lin Ma, Derek B. Ingham, Mohamed Pourkashanian

Centre for Computational Fluid Dynamics, University of Leeds, Leeds, UK

ARTICLE INFO

Article history:
Received 28 August 2009
Received in revised form
20 December 2009
Accepted 17 January 2010
Available online 28 January 2010

Keywords:
Multicomponent mass transport
Solid oxide fuel cell
Stefan–Maxwell model
Dusty Gas model
Binary Friction model
Modeling

ABSTRACT

In this study, multicomponent mass diffusion models, namely the Stefan–Maxwell model (SMM), the Dusty Gas model (DGM) and the Binary Friction model (BFM) have been compared in terms of their predictive capabilities of the concentration polarization of an anode supported solid oxide fuel cell (SOFC) anode. The results show that other than the pore diameter, current density and concentration of reactants, which have a high importance in concentration polarization predictions, the tortuosity (or porosity/tortuosity) term, has a substantial effect on the model predictions. Contrary to the previous discussions in the literature, for the fitted value of tortuosities, SMM and DGM predictions are similar, even for an average pore radius as small as 2.6e−07 and current density as high as 1.5 A cm^{-2}. Also it is shown that the BFM predictions are similar to DGM for the case investigated in this study. Moreover, in this study, the effect of the pressure gradient term in the DGM and the BFM has been investigated by including and excluding this term from the model equations. It is shown that for the case investigated and model assumptions used in this study, the terms including the pressure coefficient have an insignificant effect on the predictions of both DGM and BFM and therefore they can be neglected.

1. Introduction

SOFC is a high temperature fuel cell which operates at a temperature between 500 and 1000 °C. This relatively high temperature is required as the conductance of the YSZ electrolyte increases at elevated temperatures. In recent years, attention on the intermediate temperature SOFCs that operate at a temperature less than 800 °C, increases mainly due to their advantages, such as the requirement of low cost materials, reduced thermal stresses and increased reliability. In this type of fuel cell, a thin electrolyte (5–20 μm [1]) is used to overcome the overpotential due to the reduced temperature. On the other hand, to make the cell mechanically stable, a thick anode or cathode support is required. However, this will result in an increase in the concentration overpotential due to the difficulties in the diffusion of reactants to the reaction site of the cell. Anode supported designs are more popular compared to the cathode supported design, and this is mainly due to the anode binary diffusion coefficients $D_{H_2-H_2O}$ being about four times that of the cathode counterpart, $D_{O_2-N_2}$. Hence the cathode would have a much larger concentration polarization than that of the anode for a similar thickness, porosity and the tortuosity [1].

The ordinary and the Knudsen diffusion are the two types of diffusion that generally dominate in porous medium. In ordinary diffusion, molecule–molecule interactions are important, while for the Knudsen diffusion the wall–molecule collision dominates and molecule–molecule collisions are ignored. In real cases, diffusion is probably in an intermediate state between these two limiting cases [2]. The usual approximate criterion for Knudsen diffusion is that the mean free path of the gas molecules (λ) be much larger than some characteristic dimension of the apparatus (H) (the pore diameter in the case of porous media), and for normal diffusion that the mean free path be smaller than the characteristic apparatus dimension, i.e. $Kn = \lambda/H$. Based on the value of Kn, transport phenomena in general can be classified into the continuum ($0 < Kn < 0.001$), slip ($0.001 < Kn < 0.1$), transition ($0.1 < Kn < 10$) and free-molecular ($Kn > 10$) regimes [3]. In a SOFC, the value of λ typically lies in the range 0.1–1 μm. In comparison, the pore diameter, d, is of the order of 2 μm or greater in the support material and 1 μm or less in the anode and catalyst layers. This means that both the Knudsen and molecular diffusion play an important role and the flow is in the transition region [4].

There are different multicomponent diffusion models in the chemical engineering literature, e.g. the SMM, DGM, BFM, etc. The Ficks model (FM) which is the oldest approach to predict the diffusion however is applicable for binary mixtures or dilute solutions

* Corresponding author at: Centre for Computational Fluid Dynamics, University of Leeds, School of Process, Environment and Materials Engineering, Houldsworth Building, Leeds LS2 9JT, United Kingdom. Tel.: +44 07813766039; fax: +44 0113 246 7310.
E-mail address: pmyv@leeds.ac.uk (Y. Vural).

0378-7753/$ – see front matter © 2010 Elsevier B.V. All rights reserved.
doi:10.1016/j.jpowsour.2010.01.033

Nomenclature

N_i	molar flux of species i (mol m^{-2} s^{-1})
J_i	molar diffusion flux of species i (mol m^{-2} s^{-1})
x_i	molar fractions of components i
N_T	total molar flux of species i (mol m^{-2} s^{-1})
c_i	molar density of species i (mol m^{-3})
c_T	total concentration of gas mixture (kg m^{-3})
x_i	molar fractions of components i
D_{ij}	binary diffusion coefficient (m^2 s^{-1})
f_{im}^{BFM}	wall friction coefficient of the BFM
K_p	channel permeability (m^2)
κ_i	coefficient as a function of the partial viscosity and partial pressure (s)
η_{conc}	concentration polarization
ε	porosity
τ	tortuosity
τ^2	tortuosity factor
T	temperature (K)
P	pressure (Pa)
P_i	partial pressure of species i (Pa)
r	average pore radius (m)
R	universal gas constant (=8.314) (J mol^{-1} K^{-1})
C	constant (=1.03 × 10^{-2})
T	temperature (K)
V_i	molecular diffusion volumes of species i
$D_{i,Kn}$	Knudsen diffusion coefficient of species i (m^2 s^{-1})
M_i	molar weight of species i (kg mol^{-1})
B_o	intrinsic permeability (m^2)
η_i^0	pure-component viscosity of component i (μP)
σ	hard sphere diameter (A^0)
Ω_v	temperature dependent collision integral

and not for multicomponent mixtures. Therefore it is not discussed further in this study. The SMM takes into account the interaction among the molecules through the collision of the molecules with each other. DGM, which is also called as the extended SMM in the literature, takes into account the Knudsen diffusion, which is an important phenomenon especially in a medium consisting of small pores. In recent years, Kerkhof [5] criticized the DGM and argued that the addition of a viscous flux to the friction equations, as performed in the DGM, is erroneous because the viscous friction has already been accounted for in the equations before the addition [5]. Based on the discussion, he derived a new multicomponent model, namely the BFM. The other difference between the BFM and the DGM is the inclusion of the diffusive slip as well as the viscous slip phenomena (see [5,6]). The computational requirement for the BFM is much more extensive than the DGM, and that of the DGM is more demanding than the SMM. In recent years, in the fuel cell literature, BFM also gained increasingly more attention and this work was modified and extended for fuel cells by Young and Todd [7] and Fimrite et al. [8]. However, there is still no extensive research that shows the advantages of the BFM over the DGM in comparison with the experimental data in porous medium. It is still an open question as to which multicomponent mass transfer model to use to accurately predict the multicomponent diffusion in the porous electrodes as well as in the gas channels of fuel cells.

Suwawarangkul et al. [9] compared the modified FM, SMM and the DGM for their predictive capabilities of the models in terms of their prediction of the concentration overpotential for an anode supported planar type SOFC anode for the binary CO–CO_2 and the ternary H_2–H_2O–Ar components. They compared the models using the experimental data of Yakabe et al. [10]. To the authors' knowledge, this is the first and only available direct measurement of the concentration overpotential for SOFCs. Their conclusion was that that DGM predicts the model results the best, especially for the small pore diameter medium, at high current densities and low reactant concentration. They presented the results in the table form indicating the pore diameters only for the CO–CO_2 system and not for the H_2–H_2O–Ar system. However, the solution for the ternary mixtures appears to be problematic as the presented prediction of the models fail to accurately predict the concentration polarization and also a detailed discussion of the results is not given for ternary mixtures. The work of Suwawarangkul et al. [9] can be criticized on two accounts. Firstly, for the solution of the ternary mixtures equations for SMM and DGM, the mole fraction of Ar was assumed constant in the solution. In fact, the change in the mole fractions of the other species causes a change in Ar, even if Ar is an inert gas and the its molar flux is zero at the triple phase boundary (TPB) and through the anode and gas channel domain in the one-dimensional solution. This point is discussed more thoroughly in this paper. Secondly, the tortuosity parameter, which is used as a fit parameter following the work of Yakabe et al. [10] was assumed to take the same value in all the models. In fact, since it is a fit parameter it must be fitted to the best value for each model individually.

Tseronis et al. [11] extended the study of Suwawarangkul et al. [9] to the two-dimensional case. They compared the SMM and DGM for the 1D and 2D cases for the H_2–H_2O–Ar ternary system. Their results were in agreement with the results of Suwawarangkul et al. [9] and also they showed that the 2D predictions improve compared with the 1D result, especially at high current densities and low concentration regions. In their work, they again ignored the effect of the tortuosity parameter on the results and same value of this parameter was used as in [9]. Different from the model equations of the DGM used in Suwawarangkul et al. [9], Tseronis et al. [11] considered the pressure gradient term in the DGM equations.

In this study, the three different multicomponent diffusion models, namely the SMM, DGM and BFM are compared in terms of their prediction performance of concentration polarization of a SOFC anode. In contrast to the previous work, the effect of the tortuosity on the model comparison results is discussed. The model equations are solved for the one-dimensional case for both the uniform and non-uniform pressure terms in the DGM and the BFM equations.

2. Definition of the system

The experimental data of Yakabe et al. [10] has been used in this study. The concentration polarization at 0.3, 0.7 and 1.0 A cm^{-2} was measured for the H_2–H_2O–Ar ternary gas system and the CO–CO_2 binary gas system. Fig. 1 is a schematic diagram of the anode supported SOFC system on which the experiments were performed. For more details of the system, see [10].

In the measurements, the cell operating temperature was maintained at 750 °C. In addition to the cell temperature, the current densities were assumed to be uniform over the entire electrolyte/anode interface. The value of η_0 is the concentration overpotential at $CO/(CO + CO_2) = 0.64$ for CO–CO_2 binary system and at $H_2/(H_2 + H_2O + Ar) = 0.8$ for H_2–H_2O–Ar ternary system. The calculated η_c is the average value over the anode–electrolyte triple phase boundary (TPB) (see [10] for details of the experiment). The same parameters as employed in [10] are used in this study (see Table 1). The tortuosity factor was found by fitting the experimental data of Yakabe et al. [10] and found to be 4.5. The same value was also used by Suwawarangkul et al. [9] and it is initially used in this study. Its value is then changed and the effects are discussed further.

In this study, following the work of Yakabe et al. [10], the 3D system (Fig. 1) is simplified into a 1D system (Fig. 2), and the

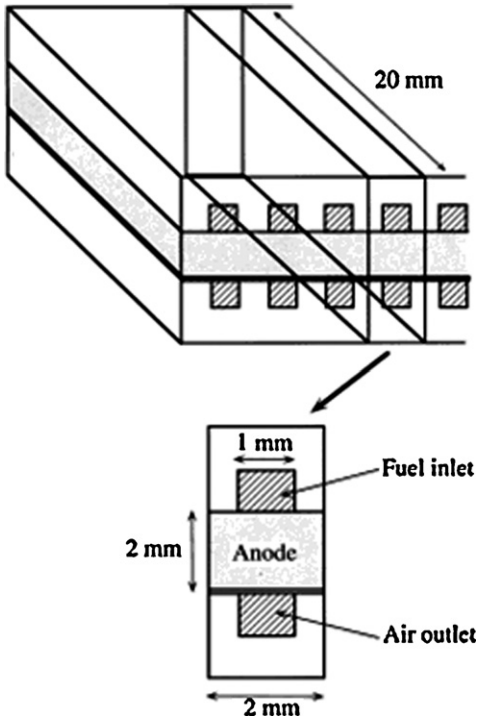

Fig. 1. Schematic diagram of the one cell stack and the single-unit cell model for the anode supported SOFC [10].

model equations are solved for the anode porous medium in the z-direction, and the molar fractions calculated at the reaction site (TPB).

3. Methodology

3.1. Conservation equation

The molar conservation equation of species i in 1D is given by:

$$\frac{\partial c_i}{\partial t} - \frac{\partial (N_i)}{\partial z} = 0 \quad \text{for } i = 1, 2, \ldots, n \quad \text{mol m}^{-3}\,\text{s}^{-1} \tag{1}$$

Table 1
Model parameters [10].

Parameter	Value	Unit
Temperature (T)	1023	K
Pressure (P)	10^5	Pa
Universal gas constant (R)	8.314	J mol^{-1} K^{-1}
Average pore radius (r)	2.6e−06	m
Porosity (ε)	0.46	–
Anode thickness (z)	2e−03	m
Anode permability	1.7e−10	m^2 Pa^{-1} s^{-1}

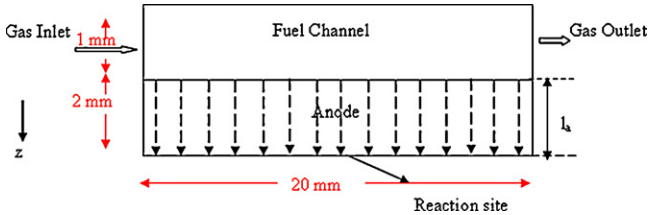

Fig. 2. Schematic diagram of the SOFC geometry used in the model development Suwanwarangkul et al. [9].

where N_i is the molar flux and related to the molar diffusion flux by [12]:

$$N_i = J_i + c_i u = J_i + N_T x_i \tag{2}$$

where N_i the molar flux of species i (mol m^{-2} s^{-1}); J_i the molar diffusion flux of species i (mol m^{-2} s^{-1}); x_i the molar fractions of components i (–) and $\sum_{i=1}^{N} x_i = 1.0$; N_T the total molar flux of species i (mol m^{-2} s^{-1}) and $\sum_{i=1}^{N} N_i = N_T$; c_i the molar density of species i (mol m^{-3}).

By inserting Eq. (2) into Eq. (1), Eq. (1) can be rewritten as follows:

$$\frac{\partial c_i}{\partial t} - \frac{\partial (c_i u + J_i)}{\partial z} = 0 \tag{3}$$

Eq. (3) for a steady state system, i.e. $\partial c_i/\partial t = 0$, and ignoring the viscous term, $c_i v$, gives:

$$\frac{dJ_i}{dz} = \frac{dN_i}{dz} = 0 \tag{4}$$

In the following section, the models to solve for N_i are presented and the solutions are discussed in detail.

3.2. Multicomponent diffusion models

3.2.1. Stefan–Maxwell model (SMM)

The steady state, isothermal multicomponent diffusion equation according to Stefan–Maxwell is given by

$$\sum_{\substack{j=1 \\ j \neq i}} \frac{N_i x_j - N_j x_i}{D_{ij}} = -c_T \nabla x_i \quad i = 1, 2, \ldots, n \quad (\text{mol m}^{-4}) \tag{5}$$

where c_T the total concentration of gas mixture (kg m^{-3}); x_i the molar fractions of components i [–]; N_i the molar flux of species i (mol m^{-2} s^{-1}); D_{ij} the binary diffusion coefficient (m^2 s^{-1}).

For ideal gases $c_T = P(RT)$, where R is the universal gas constant (J mol^{-1} K^{-1}), P is pressure (Pa) and T is temperature (K). A full derivation of Eq. (5) can be found in any multicomponent transfer book, for example Ref. [12], and therefore this aspect is not discussed any further. Since the sum of the mole fractions sum to 1.0 (or ∇x_i sum to zero), the $n-1$ equation is independent, and the nth component gradient is given by [12]:

$$\nabla x_n = -\nabla x_1 - \nabla x_2 - \cdots - \nabla x_{n-1} \tag{6}$$

In the SOFC anode, the component fluxes at the triple phase boundary are given by:

$$N_1 = -\frac{i}{nF}; \quad N_2 = \frac{i}{nF} \text{ and } N_3 = 0 \tag{7}$$

where 1, 2 and 3 refer to H_2, H_2O and Ar, respectively. In steady one-dimension, and ignoring the viscous term, Eq. (4) suggests that N_i is constant over the anode domain and therefore the flux of each component written above are the flux of the equations for the models. For example, for the SMM for the ternary mixture where $N_3 = 0$, the set of equations reduce to:

$$\begin{aligned} \frac{N_1 x_2 - N_2 x_1}{D_{12}} + \frac{N_1 x_3}{D_{13}} &= -c_T \frac{dx_1}{dz} \\ \frac{N_2 x_1 - N_1 x_2}{D_{12}} + \frac{N_2 x_3}{D_{23}} &= -c_T \frac{dx_2}{dz} \\ -\frac{N_1 x_3}{D_{13}} + -\frac{N_2 x_3}{D_{23}} &= -c_T \frac{dx_3}{dz} \end{aligned} \tag{8}$$

For known boundary conditions at the inlet $x_1 = x_{bulk}$, and for a constant N_i, the solution can be found analytically.

3.2.2. Dusty Gas model (DGM)

The physical picture behind the model is that of a dusty gas in which the dust particles constitute the porous medium. The array of dust particles is treated as one component of the gas mixture, consisting of giant, heavy molecules that are motionless and uniformly distributed in space. If there are any pressure gradients in the gas, an external force must be exerted on the dust particles to keep them motionless [13]. The governing equations were first written including the dust particles, and then the terms relating to the dust particles have been eliminated from the equations.

DGM equations are given by [14]:

$$\frac{N_i}{D^e_{i,Kn}} + \sum_{j\neq i}\frac{x_jN_i - x_iN_j}{D^e_{ij}} = -\frac{P}{RT}\nabla x_i - \frac{x_i}{RT}\left(1 + \frac{B_oP}{\mu D^e_{i,Kn}}\right)\nabla P \tag{9}$$

At a uniform pressure, the DGM equations are solved using the approach described above for SMM. At a non-uniform pressure, we follow the same approach as Zhu and Kee [15]. By summing the equation over the n components, the second term on the left hand side of Eq. (9) vanishes and the first term on the right hand side of Eq. (9) is equal to zero since $\nabla\left(\sum x_i\right) = 0$ and we obtain:

$$-\nabla P = \frac{\sum \frac{N_i}{D^e_i}}{\frac{1}{RT} + \sum \frac{x_i}{RT}\frac{B_oP}{\mu D^e_{i,Kn}}} \tag{10}$$

If Eq. (10) is inserted into Eq. (9), we obtain:

$$\frac{N_i}{D^e_i} + \sum_{j\neq i}\frac{x_jN_i - x_iN_j}{D^e_{ij}} = -\frac{P}{RT}\nabla x_i + \frac{x_i}{RT}\left(1 + \frac{B_oP}{\mu D^e_{i,Kn}}\right)\frac{\sum \frac{N_i}{D^e_i}}{\frac{1}{RT} + \sum \frac{x_i}{RT}\frac{B_oP}{\mu D^e_{i,Kn}}} \tag{11}$$

If the equations are written for ternary mixtures, the following final equations for each species are obtained:

$$\nabla x_1 = -\frac{RT}{P}\left(\frac{N_1}{D^e_1} + \frac{x_2N_1 - x_1N_2}{D^e_{12}} + \frac{x_3N_1 - x_1N_3}{D^e_{13}} - \frac{x_1}{RT}\left(1 + \frac{B_oP}{\mu D^e_{1,Kn}}\right)\left(\frac{\frac{N_1}{D^e_{1,Kn}} + \frac{N_2}{D^e_{2,Kn}} + \frac{N_3}{D^e_{3,Kn}}}{\frac{1}{RT} + \frac{x_1}{RT}\frac{B_oP}{\mu D^e_{1,Kn}} + \frac{x_2}{RT}\frac{B_oP}{\mu D^e_{2,Kn}} + \frac{x_3}{RT}\frac{B_oP}{\mu D^e_{3,Kn}}}\right)\right) \tag{12}$$

$$\nabla x_2 = -\frac{RT}{P}\left(\frac{N_2}{D^e_{2,Kn}} + \frac{x_1N_2 - x_2N_1}{D^e_{21}} + \frac{x_3N_2 - x_2N_3}{D^e_{23}} - \frac{x_2}{RT}\left(1 + \frac{B_oP}{\mu D^e_{2,Kn}}\right)\left(\frac{\frac{N_1}{D^e_{1,Kn}} + \frac{N_2}{D^e_{2,Kn}} + \frac{N_3}{D^e_{3,Kn}}}{\frac{1}{RT} + \frac{x_1}{RT}\frac{B_oP}{\mu D^e_{1,Kn}} + \frac{x_2}{RT}\frac{B_oP}{\mu D^e_{2,Kn}} + \frac{x_3}{RT}\frac{B_oP}{\mu D^e_{3,Kn}}}\right)\right) \tag{13}$$

The solutions for x_1 and x_2 at the TPB were obtained with the given boundary conditions for x_1 and x_2 at the inlet (bulk) and known N_1 and N_2 (Eq. (9)). The final component, x_3, was calculated by using Eq. (6). The solutions were obtained using MATLAB.

3.2.3. Binary Friction model (BFM)

The final set of equations for the general n-component in 1D is given by [16]:

$$-\frac{dP_i}{dz} = \frac{\tau^2}{\varepsilon}\left[\sum RT\frac{N_ix_j - N_jx_i}{D_{ij}} + f^{\mathrm{BFM}}_{im}RTN_i\right] \tag{14}$$

where f^{BFM}_{im} the wall friction coefficient of the BFM and defined as follows:

$$f^{\mathrm{BFM}}_{im} = \left(D^K_i + \frac{K_p}{\kappa_i}\right)^{-1} \tag{15}$$

where K_p the channel permeability (m^2); κ_i the coefficient as a function of the partial viscosity and partial pressure (s)

$$D^K_i = 0.89 \cdot D_{i,Kn}$$

where D^K_0 the Knudsen diffusion coefficient. The calculation is described in the following subsection.

$$\kappa_i = \frac{\eta_i}{x_ip} = \frac{1}{p}\frac{\eta^o_i}{\sum_{j=1}^{n} x_j\varepsilon_{ij}}\ (s) \tag{16}$$

where

$$\eta_i = \frac{x_i\eta^o_i}{\sum_{j=1}^{n} x_j\varepsilon_{ij}} \tag{17}$$

and

$$\varepsilon_{ij} = \frac{\left[1 + (\eta^0_i/\eta^0_j)^{1/2}\left(M_{w,j}/M_{w,i}\right)^{1/4}\right]^2}{\left[8(1 + M_{w,i}/M_{w,j})\right]^{1/2}} \tag{18}$$

η^0_i the pure-component viscosities of the components at the prevailing temperature.

It should be noted that the tortuosity and porosity terms are added following the approach of Epstein [17]. This states that instead of multiplying the binary diffusion coefficient by ε/τ in the SMM and DGM, the flux, N is multiplied by τ^2/ε. In fact, at uniform pressure, for the BFM, this means the multiplication of the binary diffusion coefficient with ε/τ^2. Hence τ in the DGM and SMM corresponds to τ^2 in the BFM. For further details, see [17].

Eq. (14) can be written as follows:

$$-x_i\frac{dP}{dz} - P\frac{dx_i}{dz} = \frac{\tau^2}{\varepsilon}\left[\sum RT\frac{N_ix_j - N_jx_i}{D_{ij}} + f^{\mathrm{BFM}}_{im}RTN_i\right] \tag{19}$$

Since the derivation of the BFM starts from defining the flux equations for a capillary and transferring it to the porous medium, N_i is defined as the average flux term over the radius of the capillary.

When Eq. (19) is written and added for each species i, the SMM term (first term on the right hand side of Eq. (19)) cancel out:

$$-\frac{dP}{dz} = \frac{\tau^2}{\varepsilon}\left[\sum f^{\mathrm{BFM}}_{im}RTN_i\right] \tag{20}$$

If Eq. (20) is inserted into Eq. (19), we obtain:

$$\frac{dx_i}{dz} = -\frac{1}{P}\left[\frac{\tau^2}{\varepsilon}\left[\sum RT\frac{N_ix_j - N_jx_i}{D_{ij}} + f^{\mathrm{BFM}}_{im}RTN_i\right] + x_i\frac{dP}{dz}\right] \tag{21}$$

The solution procedure for the BFM at the uniform and the non-uniform pressure is the same as that described in the preceding section for the DGM.

3.2.4. Calculation of the concentration polarization

Concentration polarization is the loss of the cell voltage due to the limitations associated with the diffusion of the reactants to the reaction site, i.e. electrode–electrolyte–reactant triple phase boundary (TPB). After calculation of the mole concentrations of the

species at the TPB using any of the models described above, the concentration polarization is calculated accordingly [1]:

$$\eta_{\text{conc}} = -\frac{RT}{2F}\ln\left(\frac{P_{H_2,\text{TPB}}P_{H_2O,\text{bulk}}}{P_{H_2,\text{bulk}}P_{H_2O,\text{TPB}}}\right) \quad (22)$$

where $P_{i,\text{TPB}}$ and $P_{i,\text{bulk}}$ are the partial pressures of the species i at the TPB and the bulk, respectively, and is the multiplication of mole fraction of the species i by pressure: $P_i = x_i \cdot P$.

3.3. Comparison of the models

In general, the SMM can be applied to multicomponent diffusion problems. However, the SMM does not take the Knudsen diffusion term into account for the pore size effect. The DGM is computationally more demanding than the SMM. The flux ratio is determined using the Graham law of diffusion in gaseous mixtures. The BFM was derived to predict the multicomponent diffusion flux in the transition region after defining the erroneous terms in the derivation of DGM. However, it is computationally more demanding than DGM. Moreover, the final set of equations does not satisfy the Graham law for diffusion at zero pressure gradients.

If the models above are evaluated in terms of the performance in the prediction of species transport in the porous electrodes of fuel cells, the models which take into account the effect of the molecule wall collision are expected to give a better performance, since the wall–molecule interactions play an important role in the diffusion processes that occur in the small pores of porous electrodes of the fuel cell. The DGM and BFM take into account this phenomenon. However, in contrast to DGM, BFM takes into account the diffusion slip phenomena. The model equations of the BFM have been formulated first for a capillary tube, and for the porous medium, the parameters ε and τ parameters are introduced. The DGM and SMM absorb the ε/τ term into the diffusivities while the BFM has followed the work of Epstein [15], and inserted the τ^2/ε term into the flux. If the models are evaluated in terms of their computational ease, then SMM appears to be the simplest approach, whereas more computational effort is required to solve DGM and even more for the BFM. The closure equation of SMM is that the total flux is zero (i.e. $\sum_i N_i = 0$). However DGM satisfies the Graham Law at uniform pressure and the BFM does not satisfy either the Graham law or the total zero flux condition.

3.4. Model assumptions

The assumptions of the model are consistent with those of Suwawarangkul et al. [9], except that in this study both the uniform and non-uniform model equations are used. They are listed as follows:

- Ideal gas assumption which is accurate at low pressures and high temperatures when the density is low.
- Isothermal system.
- Species concentrations were assumed constant along the gas channel and hence only the porous gas diffusion layer was considered in the 1D analysis (see also [9]).
- Steady state analysis.
- The electrochemical reactions are assumed to take place only at the anode–electrolyte interface.

3.5. Model parameters

The model parameters are those as used in the experimental work of Yakabe et al. [10] and are given in Table 1.

The tortuosity is a fit parameter and in this study it was initially set to be 4.5 as this was the value used in the previous studies, see [9–11]. The effect of this parameter is discussed in the subsequent sections. The estimation of the diffusion coefficients, pure-component and mixture viscosity and permeability are discussed in the following section.

3.6. Parameter estimation

3.6.1. Binary diffusion coefficient

In this study, binary diffusion coefficients are calculated using the Fuller et al. theory [12]:

$$D_{12} = CT^{1.75}\frac{\sqrt{\left\{(M_1+M_2)/M_1M_2\right\}}}{P\left\{\sqrt[3]{V_1}+\sqrt[3]{V_2}\right\}^2} \quad (23)$$

where D_{12} the binary diffusion coefficient ($m^2\,s^{-1}$); C the constant [1.03×10^{-2}]; T the temperature (K); P the pressure (Pa); M_1 and M_2 the molar weight ($g\,mol^{-1}$); V_1 and V_2 the molecular diffusion volumes [−]; the V_i value is obtained from [12], Table 4.1.

The effective diffusion coefficient in the SMM and DGM is calculated by introducing the porosity (ε) over tortuosity (τ) term as follows:

$$D_{ij,\text{eff}} = \frac{\varepsilon}{\tau}D_{ij} \quad (24)$$

3.6.2. Knudsen diffusion coefficient

From kinetic theory, the Knudsen diffusion coefficient, $D_{i,Kn}$ is given by [18]:

$$D_{i,Kn} = \frac{2}{3}r\sqrt{\frac{8R_gT}{\pi M_i}} \quad (25)$$

where $D_{i,Kn}$ the Knudsen diffusion coefficient ($m^2\,s^{-1}$); r the mean pore radius (m); M_i the molar weight ($kg\,mol^{-1}$).

The calculated diffusion coefficients for the given temperature, pore diameter and species in this study are $D_{H_2,Kn} = 0.0057\ m^2\,s^{-1}$, $D_{H_2O,Kn} = 0.0019\ m^2\,s^{-1}$, and $D_{Ar,Kn} = 0.0013\ m^2\,s^{-1}$.

3.6.3. Permeability (B_o)

The permeability of the anode was measured in Yakabe et al. [10] and it is given by $1.7e{-}10\,m^2\,Pa^{-1}\,s^{-1}$. It is stated that this value was measured using N_2 gas at room temperature. To calculate the intrinsic permability with units of m^2, the measured value must be calculated using the pure-component viscosity of N_2 ($\eta^0_{N_2}$) at 298 K. From the Chapman–Enskog equations described in detail in Section 3.6.4, $\eta_{N_2} = 1.7393e-05$ at 293 K. Hence $B_o = 1.7e-10\times1.7393e{-}05 = 2.96e{-}15\,m^2$. It should be noted that, in Tseronis et al. [11], the value of B_o is set to be $1.98e{-}10\,m^2$, but no reasons for this choice is given.

3.6.4. Pure-component viscosity and mixture viscosity

For the calculation of pure-component viscosity, η_0, the first-order Chapman–Enskog theory is used in this study and the viscosity can be written as follows [18]:

$$\eta_i^0 = \frac{26.69(M_iT)^{1/2}}{\sigma^2\Omega_v} \quad (26)$$

where η_i^0 the pure-component viscosity of component i (μP); M_i the molecular weight of component i ($g\,mol^{-1}$); T the temperature (K); σ the hard sphere diameter (A^0); Ω_v the temperature dependent collision integral.

To use this relation to estimate the viscosities, the collision diameter σ and the collision integral Ω_v must be determined.

Table 2
Calculated viscosities of different gas components at different temperatures.

Substance	$T(K)$	Calculated η^0(Pa s)
CO	1023	4.7630e−05
CO_2	1023	3.9761e−05
Ar	1023	5.2899e−05
H_2	1023	1.9846e−05
H_2O	1023	3.6614e−05
N_2	293	1.7393e−05

Neufeld et al. [19] proposed an empirical equation which is convenient for computer application [18]:

$$\Omega_v = \left[A(T^*)^{-B}\right] + C\left[\exp(-DT^*)\right] + E\left[\exp(-FT^*)\right] \quad (27)$$

where $T^* = kT/\varepsilon$, $A = 1.16145$, $B = 0.14874$, $C = 0.52487$, $D = 0.77320$, $E = 2.16178$ and $F = 2.43787$.

The calculated viscosities of the components at the corresponding temperatures are presented in Table 2.

Then the mixture viscosity was calculated using the Wilke formula [18]:

$$\eta_i = \frac{x_i \eta_i^o}{\sum_{j=1}^{n} x_j \varepsilon_{ij}} \quad (28)$$

$$\varepsilon_{ij} = \frac{\left[1 + (\eta_i^0/\eta_j^0)^{1/2}\left(M_{w,j}/M_{w,i}\right)^{1/4}\right]^2}{\left[8(1 + M_{w,i}/M_{w,j})\right]^{1/2}} \quad (29)$$

η_i^0 the pure-component viscosities of the components, at the prevailing temperature.

4. Results and discussion

4.1. Results at uniform pressure

In Fig. 3(a) and (b), the predictions of the DGM, SMM and BFM are presented for the CO–CO_2 and H_2–H_2O–Ar systems, respectively. η_0 is the concentration polarization where $H_2/(H_2 + H_2O + Ar) = 0.8$ and $CO/(CO + CO_2) = 0.64$. As expected, a decrease in the concentration leads to an increase in the concentration polarization at all current densities due to the reactant concentration deficiencies at the TPB sites where the reactions take place. On the other hand, as the current densities increase, the concentration polarization increases proportionally. Again this is the result of the high reactant consumption at the reaction site associated with the high current density withdrawal. In general, it is observed that the concentration polarization of the CO–CO_2 is higher than that of H_2–H_2O–Ar. This is due to the higher binary diffusion coefficient of CO–CO_2. Therefore the limiting current density of the cell using CO–CO_2 is much smaller than that of the H_2–H_2O–Ar system. The tortuosity was kept constant at a value of 4.5 for all the cases considered here. It should be noted that, as explained in the previous section, the tortuosity factor (τ^2) for the BFM corresponds to the tortusoity (τ) of the DGM and SMM. What is observed in the results is that for the CO–CO_2 system, in all the three models, the DGM predictions are best while the SMM is the worst, especially at high current densities and low reactant concentrations. For the H_2–H_2O–Ar system, the DGM and BFM results are quite similar, while their predictions are slightly better than the SMM prediction for the experimental data when the same tortuosity parameter (4.5) is used for all the models. These results are different from those presented by Suwarwarangkul et al. [9], especially for the ternary mixtures (see Fig. 3 in [9]). This is most probably due to the assumed constant Ar component which was discussed in the previous sections. On the other hand, the results are comparatively more similar with the 1D solution of Tseronis et al. [11]. The slight differences may be due to the numerical solver as well as the differences in the permeability and the viscosity parameters used. In this study, the mixture viscosity was calculated using the Wilke formula and this value is dependent on the species mole fractions and for the permeability of the medium the experimental data of Yakabe et al. [10] was used. In Tseronis et al. [11], however, no explanation was given for choice of the values of the viscosity and permeability which were taken to be 2.01e−05 and 1.98e−10, respectively.

At the current density 0.1 A cm^{-2}, the SMM, DGM and BFM fit the experimental data quite well. As the current density increases to 0.3 A cm^{-2}, the DGM produces a better prediction than does the SMM and BFM. At 0.5 A cm^{-2}, all the models fail to give an accurate prediction. In general, between these three models, DGM gives a better prediction than does SMM and BFM at all the current densities for the set of parameters used in this particular system. On the other hand, at $\tau = 4.5$, BFM gives the worst prediction of all three models for the CO–CO_2 system. The BFM and DGM results are similar for the H_2–H_2O–Ar system. The difference between the BFM and DGM results is in the wall friction coefficient term, f_{im}^{BFM} in the BFM. This term, which is given by $f_{im}^{BFM} = \left(0.89 \cdot D_{i,Kn} + K_p/\kappa_i\right)^{-1}$, corresponds to $(D_{i,Kn})^{-1}$ in the DGM. The calculations in this study show that K_p/κ_i are relatively smaller compared to the values of $0.89 \cdot D_i^K$. Hence the only difference between the BFM and DGM predictions is in the $0.89 \cdot D_i^K$ term.

As was emphasized previously, the solutions have been obtained by setting the tortusoity to a value of 4.5 in all the models. The

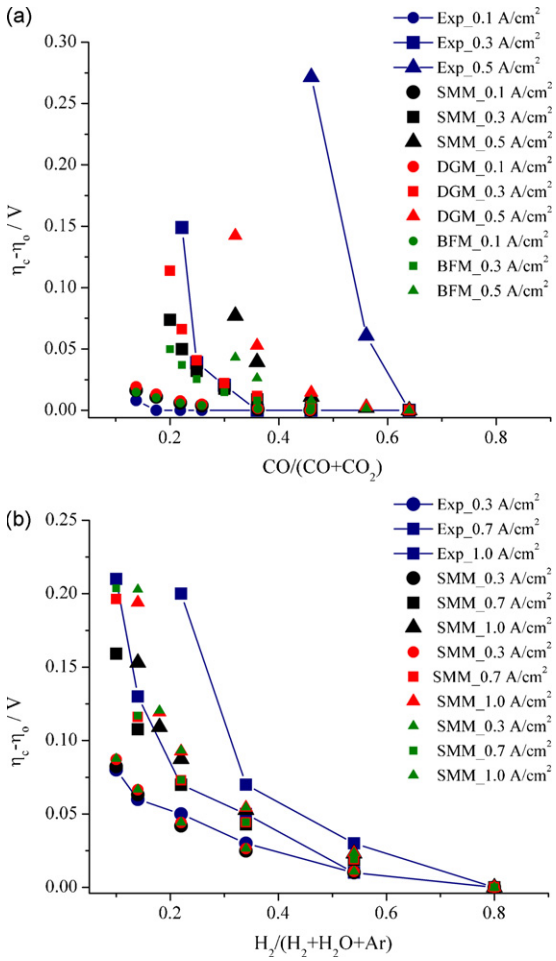

Fig. 3. DGM, SMM and BFM predictions for (a) CO–CO_2 system at 0.1, 0.3 and 0.5 A cm^{-2} and (b) H_2–H_2O–Ar system at 0.3, 0.7 and 1.0 A cm^{-2} and comparison with the experimental data (τ is 4.5 in DGM and SMM, and τ^2 is 4.5 in the BFM).

history of setting this parameter to that value dates back to Yakabe et al. [10], where it is clearly stated that the tortuosity is used as a fit parameter.

Fig. 4(a) and (b) represents the results obtained when using the SMM, DGM and the BFM with a fitted value for the tortuosity parameter for the same case as that considered in Fig. 3. The tortuosity parameter was fitted by trial and error for all the three models. By the fitted tortuosity parameter it is meant that the value of τ in the DGM and SMM and τ^2 in the BFM equations. The fitted values for the models are shown in Table 2. It is noted that the fitted tortuosity parameter for the BFM is higher than that for the SMM and DGM and this is mainly due to the effect of the multiplier 0.89.

It is observed in Fig. 4 (a) and (b) that all the model curves are shifted to the right when tortusoity increases. This means that the concentration polarization increases as the tortuosity increases at all current density values. This is due to the fact that an increase in the tortuosity obstructs the passage of the gas molecules, which results in a decrease in the concentration of the gas molecules at the TPB where the reactions take place. As a result, the concentration polarization increases and this leads to a decrease in the operational voltage. Similarly, when the tortuosity decreases, the concentration polarization increases and the curves are shifted to the left. Also it can be seen in the figures that at high current densities and low concentrations, the same increase in tortuosity leads to a larger shift of the curves compared to low current densities and high concentration regions. This shows that the effect of the change in tortuosity is more severe, especially when the current density is high and the concentration is low, i.e. when the concentration polarization is high compared with the low current density and high concentration.

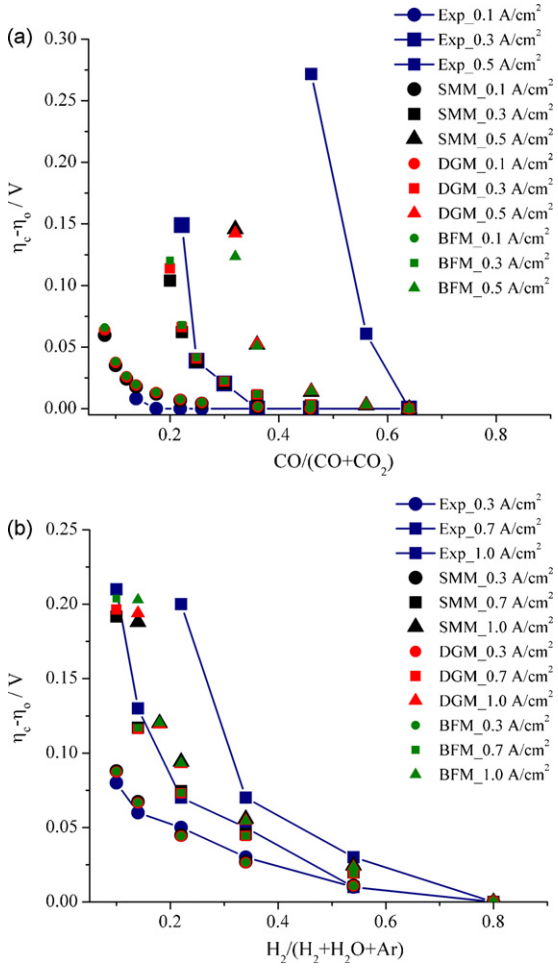

Fig. 4. DGM, SMM and BFM predictions for (a) CO–CO_2 system at 0.1, 0.3 and 0.5 A cm^{-2} and (b) H_2–H_2O–Ar system at 0.3, 0.7 and 1.0 A cm^{-2}, and comparison with the experimental data with fitted tortuosity values for each model.

Table 3
Tortuosity fitted values for the SMM, DGM and the BFM for CO–CO_2 and H_2–H_2O–Ar systems.

System	SMM	DGM	BFM
CO–CO_2	4.79	4.5	5.49
H_2–H_2O–Ar	5.0	4.5	5.29

The results presented in this section show that when the tortuosity parameter is fitted for each model, similar predictions of the concentration polarization prediction of the SMM, DGM and the BFM were obtained for the system investigated in this study. In fact, the SMM does not take into account the Knudsen diffusion, and it is clearly seen in the SMM equations that there is no term which is a function of the pore diameter. However, for the SMM, the results presented here show that the effect of the Knudsen diffusion can be compensated for by fitting the tortuosity factor. It is postulated that this is the main weakness of the study of Suwawarangskul et al. [9] and Tseronis et al. [11], where a single tortuosity factor is used for each model and comparisons have been performed accordingly.

It must be noted that according to the opinion of the authors, the reason for the poor results at high current density is that solutions were solved in only one dimension. The solution in 2D or 3D is expected to predict even more accurate results at the high current densities where the reactant concentration varies not only along the anode thickness but also along the anode length due to the high consumption of the reactants. In fact, the results of Tseronis et al. [11] also show that the model predictions improve for two-dimensional solutions, especially at high current densities and low concentrations (Table 3).

As has been discussed previously in Suwawarangkul et al. [9], the pore diameter and current density are two important factors and as the current density increases and the pore radius decreases, concentration polarization becomes dominant as the passage of the gases to the active reaction sites, i.e. TPB becomes more difficult. In fact, when the pore diameter is reduced, the Knudsen diffusion term becomes more dominant. Therefore, to investigate the extent of the validation of the results, we now extend the boundaries of the current density and the pore diameter to decide whether the model predictions are similar for a wide range of current densities and pore radii. The pore radius was decreased from 2.6e−06, to 1.6e−06, and then to 2.7e−07 with the range of current density being chosen to be 0.05, 1, and 1.5 A cm^{-2}.

4.1.1. Effect of pore radius

The pore radius is one of the most important parameters that affect the diffusion in fuel cells. Theoretically, this term is accounted for in the calculation of the Knudsen diffusion coefficient in the DGM and the BFM. In contrast, there is no term in the SMM that considers the effect of the pore radius, which means the change of the pore radius does not affect the results obtained when using the SMM.

In this section, for convenience in the presentation of the results, first the DGM is compared with that of the SMM with the experimental data with different pore sizes and then the BFM and DGM comparison is presented.

4.1.1.1. The SMM vs DGM. In Fig. 5, the concentration polarization results obtained using the SMM and DGM for the $H_2/(H_2 + H_2O + Ar)$ system at 1 A cm^{-2} are presented for the initial tortuosity parameter of 4.5 on the left hand side of the figure and the optimized tortuosity parameter on the right hand side of the figure. From

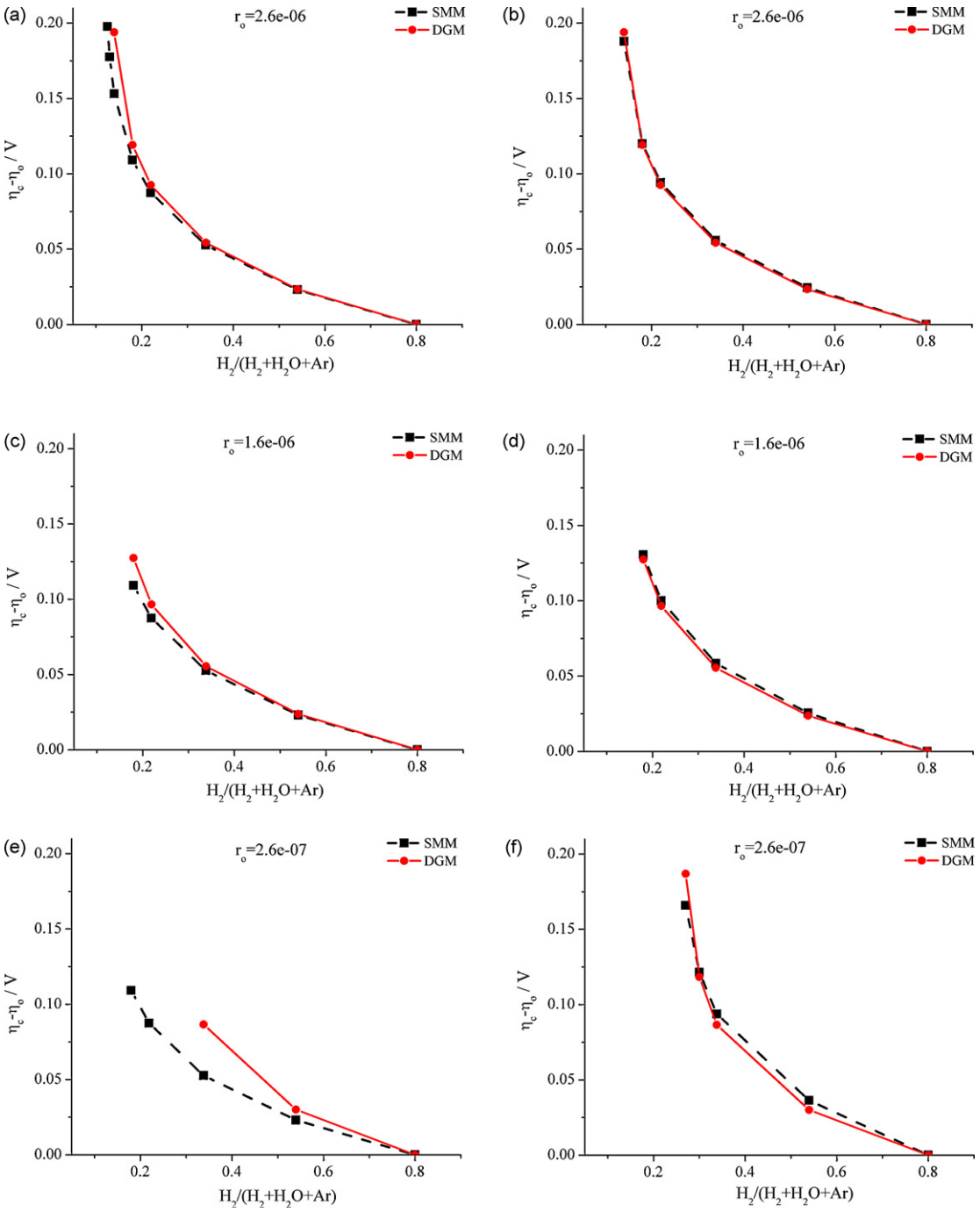

Fig. 5. The $\eta_{conc} - \eta_0$ predictions of the SMM and the DGM for the $H_2/(H_2 + H_2O + Ar)$ system at 1 A cm^{-2}; (a), (c) and (e) for pore diameters 2.6e−06, 1.6e−06 and 2.6e−07, respectively and $\tau = 4.5$ and (b), (d) and (f) same system for the optimized tortuosity parameters which are 5.0, 5.4, 10, respectively.

top to bottom, the average pore radius decreases from 2.6e−06 to 1.6e−06 and 2.6e−07 m. The highest current density of the experiment, which is 1 A cm^{-2} was selected and maintained for all the cases investigated during this analysis in order to make the analysis in the most extreme situation. In fact when the pore diameter was decreased further to 2.6e−08, we observed that the concentration polarization goes to infinity as there is no H_2 at the reaction TPB site.

It is observed that as the pore size decreases, the difference between the results obtained using SMM and DGM increases, a result which is in agreement with the theory. The flux equations of the SMM is independent of the pore radius, hence there is no change in the prediction of the SMM with the pore radius. On the other hand, when the pore diameter increases, the Knudsen term of the DGM becomes more significant. These are the initial results that we obtained with the tortuosity parameter set at a value of 4.5. On the right hand side of the figure, the results are presented when the tortusoity parameter is fitted for each model separately. The tortuosity for the DGM was kept constant at a value of 4.5 and the SMM was increased to 5.0, 5.4 and 10. The results show that the difference between the DGM and SMM in predicting the concentration polarization can be compensated for by increasing the tortuosity factor as high as twice the value as set for the DGM.

At an average pore radius 2.6e−06, the SMM produces quite similar results to the DGM, especially at high mole fractions of H_2. Only when the mole fraction is smaller than about 0.2 does a

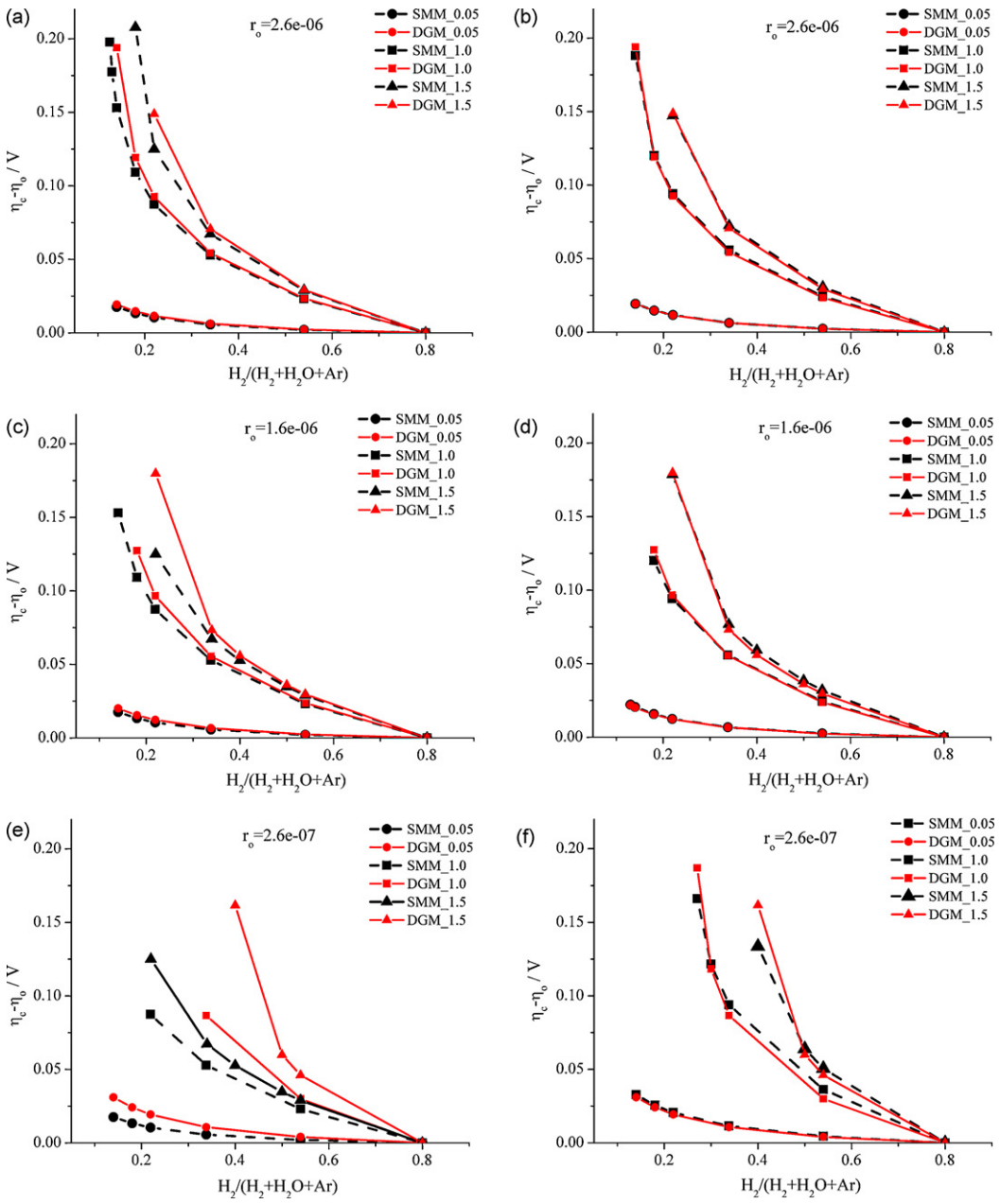

Fig. 6. The $\eta_{conc} - \eta_0$ predictions of the SMM and the DGM for the $H_2/(H_2 + H_2O + Ar)$ system at 0.05, 1, and 1.5 A cm^{-2}; (a), (c) and (e) for pore diameters 2.6e−06, 1.6e−06 and 2.6e−07, respectively and $\tau = 4.5$ and (b), (d) and (f) same system for the optimized tortuosity parameters which are 5.0, 5.4, 10, respectively.

small discrepancy between the models appear. When the tortuosity parameter was modified for the SMM to be 5.4, the SMM and DGM results match quite well. It is observed that at small pore diameters, the larger discrepancy between the SMM and DGM can be compensated by setting the tortuosity to a higher value and it is found that a value of 5.4 and 10 for pore diameters 1.6e−06 and 2.6e−07, respectively, gives quite similar predictions for the concentration polarization.

As stated in the study of Suwawarangkul et al. [9], the current density also has an important effect on the concentration polarization. That is when the current density increases, the concentration at the TPB decreases. In Fig. 6, the results are presented for each average pore radius as in Fig. 5, but for a wide range of current densities, namely 0.05, 1, and 1.5 A cm^{-2}. The results show that, even at the small pore radius, there is still a probability that the SMM produces comparatively similar results to those obtained when using the DGM by fitting the tortuosity parameter. As the pore radius decreases, and the current density increases, then the tortuosity parameter fitted for the SMM increases. Overall, for the pore diameter as small as 2.6e−07 and current density as large as 1.5 A cm^{-2}, comparatively similar agreement can be obtained for both the SMM and the DGM for the calculation of the concentration polarization. This result contradicts the conclusion of the previous research work by Suwawarangkul et al. [9] and Tseronis et al. [11].

4.1.1.2. The DGM vs BFM. In Fig. 7(a) and (b), $\eta_{conc} - \eta_0$ predictions of the DGM and BFM for the $H_2/(H_2 + H_2O + Ar)$ system at 0.05, 1, and 1.5 A cm^{-2}, pore diameters 2.6e−06 and 2.6e−07, respectively $\tau = 4.5$. In Fig. 7(b) and (d) the results for the optimized tortuosity parameters were presented.

In modeling the transport in porous medium at a uniform pressure, the theoretical difference between the DGM and the BFM

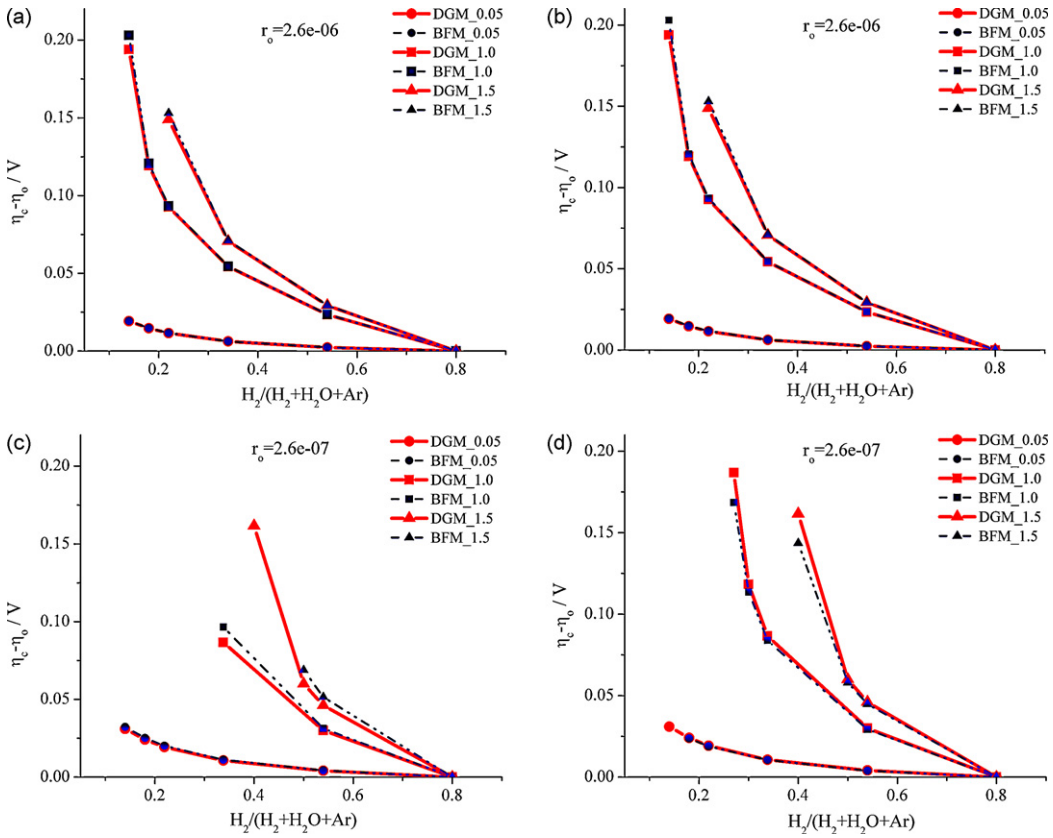

Fig. 7. The $\eta_{conc} - \eta_0$ predictions of the DGM and the BFM for the $H_2/(H_2 + H_2O + Ar)$ system at 0.05, 1, and 1.5 A cm^{-2}; (a and c) for pore diameters 2.6e−06 and 2.6e−07, respectively and $\tau = 4.5$ and (b and d) for the optimized tortuosity parameters.

is in the term called the wall friction coefficient, namely $f_{im}^{BFM} = \left(0.89 \cdot D_{i,Kn} + K_p/\kappa_i\right)^{-1}$. The results indicate that, K_p/κ_i is very small compared to the $0.89D_i^K$ value and that is be the reason for the similar predictions of the DGM and the BFM. The results are quite similar especially at small pore diameters and fitted tortuosity parameters, see Fig. 7(b) and (d).

4.1.1.3. Results at a non-uniform pressure (effect of the partial pressures in the DGM and the BFM). In the previous sections, calculations have been performed by excluding the pressure gradient in the DGM and BFM equations. This is because this term has a negligible effect when diffusion is the dominating mechanism, as in the case under investigation. In fact, in the literature, Ni et al. [20] have shown that the inclusion of this term improves the predictions of the fuel cell performance. Also one of the differences between the work of Suwararangkul et al. [9] and Tsenoris et al. [11] is that this term was included in the latter. In this section, the effect of the inclusion of this term on the predictions of DGM and the BFM in the 1D analysis are presented by calculating the predictions using Eqs. (11) and (14) for the DGM and the BFM, respectively.

In Fig. 8(a) and (b), $\eta_{conc} - \eta_0$ predictions obtained from the DGM and BFM, respectively, both with (labelled as 1) and without (labelled as 2) the additional pressure gradient term for the $H_2/(H_2 + H_2O + Ar)$ system at 0.3, 0.7, and 1 A cm^{-2} and with an average pore radius 2.6e−06. It is observed from the figure that inclusion of the partial pressure term, both in the DGM and BFM, produces a negligible effect on the results. This shows that the contribution of the additional pressure gradient term is negligibly small compared to the other terms and can, in general, be neglected in the analysis.

4.2. Further remarks and discussions on the tortuosity

Tortuosity is, in its broadest sense, the ratio of the actual path that a particle follows due the tortuous nature of the medium over the length of the medium, and by definition it is always greater than 1.0. In other words, due to the tortuous nature of the medium, the path that is travelled by a particle increases and this means a decrease in the flux. Simply this effect is taken into account by introducing the porosity, ε and the tortuosity, τ term. In a porous medium, the diffusion coefficient is usually multiplied by the factor ε/τ, which is then called the "effective" diffusion coefficient. On the other hand, Epstein [17] states that the diffusivity of a species in porous medium should be obtained by multiplication of flux of the species by the factor τ^2/ε, where τ^2 is referred to as the tortuosity factor.

In fact, the measurement of tortuosity is not as straightforward as that of the porosity. In the fuel cell literature, there is a debate on the range of values that the tortuosity parameter may take for the SOFC anode. Williford et al. [21] criticize the use of the tortuosity parameters as high as 10–17 and they found it to be in the range 2.0 and 3.0 for an anode supported SOFC anode. This range of values was obtained from the experimental data that they had collected using Stefan–Maxwell formalism. However, details of the experimentation and data analysis were not described thoroughly in the paper. Further, they noted that, depending on whether the Knudsen diffusion is taken into consideration or not, its value might vary between 2.0 and 6.0. In Jiang and Virkar [22], for different gas compositions and limiting current densities, the tortuosity varies between 5.0 and 9.0.

In fact, as stated in [21], accounting for Knudsen diffusion or not can result in different values of the tortuosity. Failure to properly account for the Knudsen effect can result in fitted tortuosities that

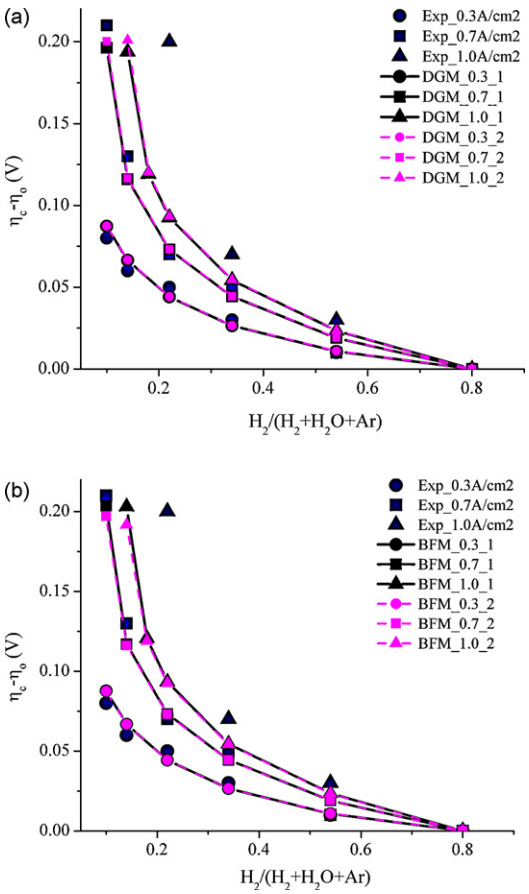

Fig. 8. $\eta_{conc} - \eta_0$ predictions of the (a) DGM and (b) BFM with and without the additional pressure gradient term, labelled as (1) and (2), respectively for the $H_2/(H_2 + H_2O + Ar)$ system at 0.3, 0.7, and 1 A cm^{-2}; for pore diameters 2.6e−06.

are about a factor two higher than the ones that take this effect into account [21]. However, Cussler [23] also states that it is hard to justify the measured quantities using geometrical arguments alone and the main advantage of using this factor is its simplicity. In fact, in this study the fitted tortuosity is in the range of 4.5–10 and thus these values are comparable to previous studies. However, it must be noted that the fluctuations in the definition of this parameter indicates that in addition to its physical meaning, the tortuosity is a convenient fit parameter used to overcome the uncertainties associated with the diffusion models. For example, in the models investigated in this study, the effect of the pore size distribution that might have an important effect in highly heterogeneous medium is not considered. Further, the surface diffusion and adsorption have been ignored and this has been mainly due to the complexity of including them and insufficient accuracy in defining these phenomena.

5. Conclusions

In this study, the performance of the SMM, DGM and the BFM has been compared in terms of their prediction capabilities of the concentration polarization in the anode of a SOFC fuel cell.

Based on this study, we can conclude as follows:

- Apart from the pore diameter and the current density, the tortuosity (or porosity/tortuosity) has a substantial effect on the predictions of concentration polarizations. Even at very high current densities (1.5 A cm^{-2}) and small pore radius (2.7e−07), for the fitted tortuosity parameter, the SMM, DGM and BFM predictions are similar, and this contradicts some of the previous studies reported in the fuel cell literature. The results show that the SMM provides a quite similar prediction of the concentration polarization (in fact at least as accurate as the DGM) with the fitted tortuosity values so it may be preferred over the DGM when considering the comparative computational ease in comparison to the DGM.
- The effect of the partial pressure has been investigated and it is concluded that the pressure gradient term in the DGM and the BFM have a very small effect on the concentration polarization predictions for the conditions investigated and hence does not need to be included in this study.
- The importance of model validation against experimental data over a wide range of conditions is demonstrated. The model appears to give a good fit in the range of the experimental operating conditions investigated but might not be appropriate at other conditions due to the empirical parameters found by fitting the model to the experimental data. Therefore the models must be validated for a large range of operating conditions before being used as a prediction tool.
- None of the 1D model gives good predictions of concentration polarization at high current densities and low fuel concentrations. The solution in 2D or 3D is expected to predict even more accurate results at high current densities where the reactant concentration varies not only along the anode thickness but also along the anode length due to the high consumption of the reactants and this will be investigated in the future. Also in the future, this work will be extended for the verification of the results obtained through comparison of the models' predictions for different cases, e.g. different fuel inlet configurations and different types of fuel cells.

Acknowledgments

Ms Vural, would like to acknowledge the European Union, European Research Commission, that is fully supporting the research work through the award of a Marie Curie EST Research Fellowship in the Centre for Computational Fluid Dynamics at the University of Leeds.

References

[1] S.C. Singhal, K. Kendall, High Temperature Solid Oxide Fuel Cells: Fundamentals, Design and Applications, Elsevier, New York, 2003.
[2] R.B. Evans, G.M. Watson, E.A. Mason, J. Chem. Phys. 35 (1961) 2076–2083.
[3] A.S. Joshi, A.A. Peracchio, K.N. Grew, K.S. Chiu, J. Phys. D: Appl. Phys. 40 (2007) 7593–7600.
[4] B.A. Haberman, J.B. Young, J. Fuel Cell Sci. Tech. 3 (2006) 312–321.
[5] P.J.A.M. Kerkhof, Chem. Eng. J. 64 (1996) 319–343.
[6] H.A. Kramers, J. Kistemaker, Physica 10 (1943) 699–713.
[7] J.B. Young, B. Todd, Int. J. Heat Mass Transfer 48 (2005) 5338–5353.
[8] J. Fimrite, B. Carnes, H. Structrup, N. Djilali, J. Electrochem. Soc. 152 (2005) A1815–A1823.
[9] R. Suwanwarangkul, E. Croiset, M.W. Fowler, P.L. Douglas, E. Entchev, M.A. Douglas, J. Power Sources 122 (2003) 9–18.
[10] H. Yakabe, M. Hishinuma, M. Uratani, Y. Matsuzaki, I. Yasuda, J. Power Sources (2000) 423–431.
[11] K. Tseronis, I.K. Kookos, C. Theodoropoulos, Chem. Eng. Sci. 63 (2008) 5626–5638.
[12] R. Taylor, R. Krishna, Multicomponent Mass Transfer, Wiley, New York, 1993.
[13] E.A. Mason, A.P. Malianuskas, Gas Transport in Porous Media: The Dusty Gas Model, Elsevier, Amsterdam, 1983.
[14] R. Jackson, Transport in Porous Catalysts, Elsevier, Amsterdam, 1977 (Chapter 5, p. 35).
[15] H. Zhu, R.J. Kee, J. Power Sources 117 (2003) 61–74.
[16] P.J.A.M. Kerkhof, M.A.M. Goebers, Chem. Eng. Sci. 60 (2005) 3129–3167.
[17] N. Epstein, Chem. Eng. Sci. 44 (1989) 777–779.

[18] B.E. Poling, J.M. Prausnitz, J.P. O'Connell, The Properties of Gases and Liquids, 5th ed., McGraw-Hill, New York, 2000.
[19] P.D. Neufeld, A.R. Janzen, R.A. Aziz, J. Chem. Phys. 57 (1972) 1100.
[20] M. Ni, D.Y.C. Leung, M.K.H. Leung, J. Power Sources 183 (2008) 668–673.
[21] R.E. Williford, L.A. Chick, G.D. Maupin, S.P. Simner, J.W. Stevenson, J. Electrochem. Soc. 150 (2003) A1067–A1072.
[22] Y. Jiang, A.V. Virkar, J. Electrochem. Soc. 150 (2003) A942–A951.
[23] E. Cussler, Diffusion: Mass Transfer in Fluid Systems, third ed., Cambridge University Press, 2009.